

## Effect of Welding Speed and Defocusing Distance on the Quality of Laser Welded Ti-6Al-4V

A.S.H. Kabir<sup>1,2</sup>, X. Cao<sup>1</sup>, M. Medraj<sup>2</sup>, P. Wanjara<sup>1</sup>, J. Cuddy<sup>3</sup> and A. Birur<sup>3</sup>

<sup>1</sup>Aerospace Manufacturing Technology Centre, Institute for Aerospace Research, National Research Council Canada, 5145 Decelles Ave., Montreal, QC, Canada, H3T 2B2

(\*Corresponding author: Xinjin.Cao@cnrc-nrc.gc.ca)

<sup>2</sup>Dept. of Mechanical and Industrial Engineering, Concordia University, 1455 De Maisonneuve Blvd. West, Montreal, Quebec, Canada, H3G 1M8

<sup>3</sup>Standard Aero Limited, 33 Allen Dyne Road, Winnipeg, Manitoba, Canada, R3H 1A1

Keywords: Nd:YAG laser, Laser welding, Ti-6Al-4V alloy

### Abstract

In this study, the weldability of 5.1-mm thick Ti-6Al-4V sheets in the mill-annealed condition was investigated using a continuous wave 4 kW Nd:YAG laser at various welding speeds and defocusing distances. The joint quality was characterized in terms of weld geometry, microstructure, defects and hardness. Although some welding defects such as underfill and porosity were observed, sound welds without cracks can be obtained using a high power Nd:YAG laser. The hardness was found to be maximum in the fusion zone (FZ) and the heat-affected zone (HAZ) near the fusion boundary, beyond which a gradual decrease occurred to the base material.

### Introduction

Ti-6Al-4V is the most widely used commercial titanium alloy in the aerospace industry and among the alpha-beta ( $\alpha$ - $\beta$ ) grades, it has the best weldability, though heating above the  $\beta$  transformation temperature during fusion welding can cause some significant changes in its structure, strength, ductility and toughness properties [1]. So far, gas tungsten arc, plasma arc [2], and electron beam welding processes [3] have been frequently used to join Ti-6Al-4V. During the past decade, laser welding has become increasingly competitive as a joining process [4] especially since the laser beam can be readily transmitted through the air and thus offers significant practical advantages over electron beam welding that conventionally requires a high vacuum environment [5, 6]. In addition, laser welding can produce a FZ and HAZ that are nearly equivalent in size to that obtained by electron beam welding and significantly less than that from gas tungsten arc welding because the high energy density of the laser beam permits the heat input to be concentrated over a very small region [1].

So far, the application of a CO<sub>2</sub> laser source has mainly been used for titanium alloys. Compared with CO<sub>2</sub> laser, Nd:YAG and fiber lasers have become more widely used in recent years [7], due to the shorter wavelength of these latter sources that result in a more stable keyhole and weld pool with a higher welding efficiency than the former [7]. In addition, the Nd:YAG and fiber lasers can be delivered to multi-workstations from one source using the fibre delivery system [8]. To date, however, very limited published work is available on the

weldability of Ti-6Al-4V using high power continuous wave (CW) solid state Nd:YAG laser. This research work forms part of a larger program on the research and technology development of welding processes for the manufacture of  $\alpha$ - $\beta$  and near- $\beta$  titanium alloys. The intent of this paper is to report on the various findings of this research work in relation to the effect of welding speed and defocusing distance on the weld quality, microstructure and mechanical properties of autogenously laser welded Ti-6Al-4V using a 4 kW CW Nd:YAG laser.

### Experimental Procedures

Grade 5 mill-annealed Ti-6Al-4V sheets with dimensions of approximately 102 in length, 63 in width and 5.1mm in thickness were laser welded autogenously along the length of the samples (perpendicular to the rolling direction). The surfaces of all the specimens were brushed and cleaned by methanol to remove any contaminants prior to the clamping and welding. A 4 kW CW solid-state Nd:YAG laser system equipped with an ABB robot and a magnetic holding fixture was used. A collimation lens of 200 mm, a focal lens of 150 mm and a fiber diameter of 0.6 mm were employed to produce a focusing spot diameter of approximately 0.45 mm. High purity argon at a flow rate of 23.6 l/min (50 cfh) was used to shield the top surface of the work-piece while the bottom surface was shielded using a mixture of 50% helium and 50% argon at a flow rate of 66.1 l/min (140 cfh) with a provision for a trail of the top surface. The samples were welded at various welding speeds at a laser power of 4.0 kW and defocusing distances of -1 mm and -2 mm (Table 1).

**Table 1 processing parameters used in this study**

Specimen #	Laser power (kW)	Welding speed (m/min)	Defocusing (mm)
T1	4.0	0.75	-1
T2	4.0	1.00	-1
T3	4.0	1.50	-1
T4	4.0	1.75	-1
T5	4.0	2.00	-1
T6	4.0	0.75	-2
T7	4.0	1.00	-2
T8	4.0	1.50	-2

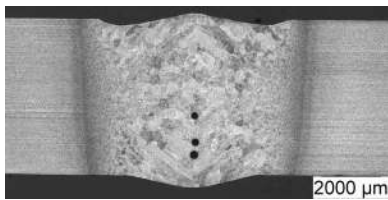
After welding, preparation for metallographic examination and analysis involved extracting specimens from the butt joints by sectioning transverse to the welding direction. The specimens were mounted using cold-setting epoxy resin, ground and polished to produce a mirror-like finish. The microstructure was revealed by using Kroll's reagent (1-3 mL HF + 2-6 mL HNO<sub>3</sub> + 100 mL H<sub>2</sub>O) for 6 – 10 s, depending on the zones of interest. Microstructural examination was carried out using an inverted metallurgical microscope (Olympus GX71) equipped with an Olympus digital camera (XC50) and AnalySIS Five digital imaging software. For each condition, at least three weld cross-sections were analyzed to obtain joint dimensions including FZ width and area, HAZ area, underfill area, maximum underfill depth and porosity area. The microindentation hardness profiles across the welded plates were measured using a 500 g test load and a dwell period of 15 seconds with a Vickers micro-hardness machine (Struers Duramin A300) having a fully automated testing cycle. For each weld condition, three hardness profiles across the weld joint, i.e. near the top, center and root height, were made with an indent

interval of 0.2 mm. It is noteworthy that this indent interval meets the minimum spacing requirement according to ASTM standards [9].

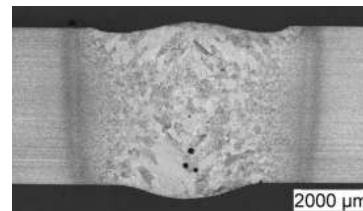
## Results and Discussion

### Weld Geometry

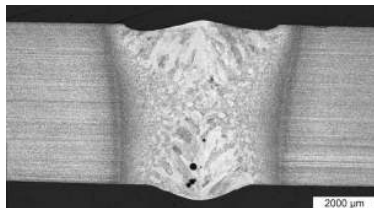
The effects of welding speed and defocusing distance on the weld geometry have been investigated at a laser power of 4 kW and at defocusing distances of -1 mm and -2 mm. Figure 1 shows the effect of welding speed and defocusing distance on the weld transverse sections. Fully penetrated welds were obtained at welding speeds from 0.75 m/min to 1.75 m/min. It was observed that the FZ width was relatively wide at 0.75 m/min and evolved with increasing welding speed to render a narrow FZ root at 1.75 m/min. At lower welding speeds, keyhole instability and collapse contributed to the formation of porosity and at the extreme limit the changeover from keyhole to conduction welding mode imparts a marked reduction in the energy density that thus renders a large weld bead profile. In contrast, at high welding speeds, a lack of penetration (LOP) occurs, as indicated in Figure 1h for 2.0 m/min.



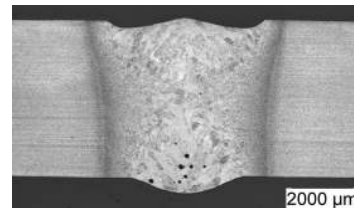
(a) Defocusing = -1 mm (0.75 m/min)



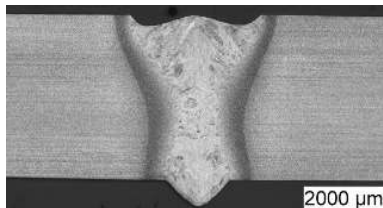
(b) Defocusing = -2 mm (0.75 m/min)



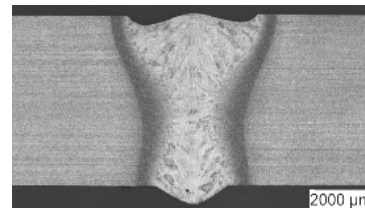
(c) Defocusing = -1 mm (1.0 m/min)



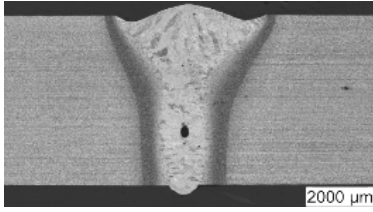
(d) Defocusing = -2 mm (1.0 m/min)



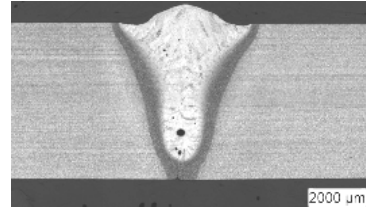
(e) Defocusing = -1 mm (1.5 m/min)



(f) Defocusing = -2 mm (1.5 m/min)



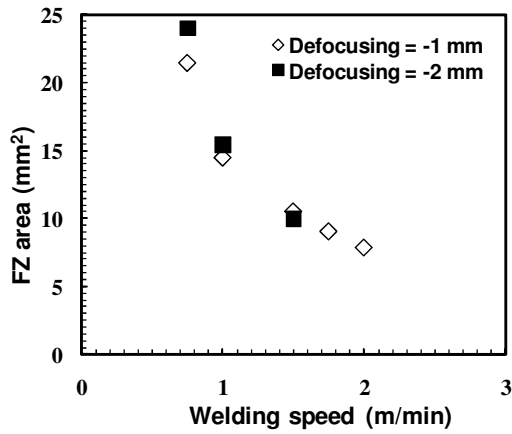
(g) Defocusing = -1 mm (1.75 m/min)



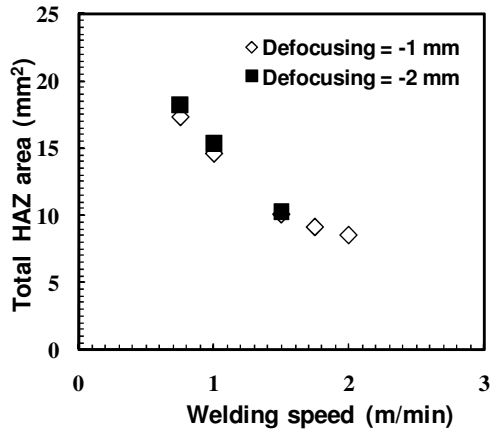
(h) Defocusing = -1 mm (2.0 m/min)

Figure 1 Transverse sections obtained at various welding speeds and defocusing distances

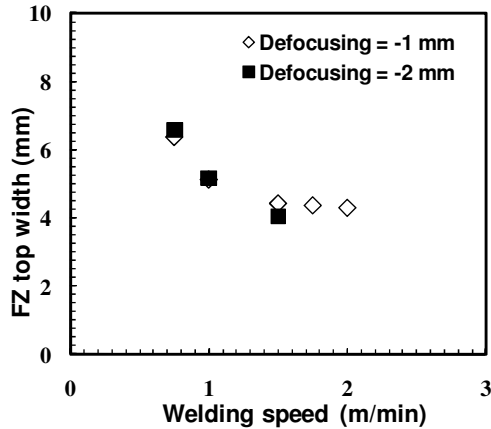
The influence of welding speed and defocusing distance on the weld bead characteristics is given Figure 2. The area of the FZ and HAZ as well as the FZ width at top, middle and root of the weld decreased with increasing welding speed. However, no significant difference in the joint dimensions has been found at the two defocusing distances (-1 and -2 mm).



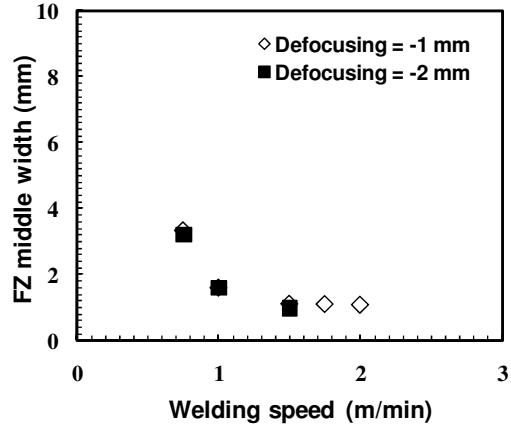
(a)



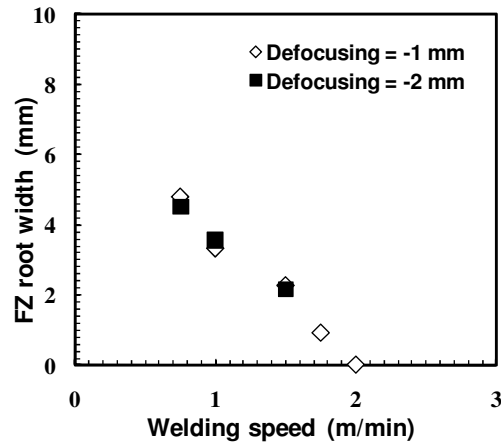
(b)



(c)



(d)



(e)

Figure 2 Effect of welding speed and defocusing distance on the FZ and HAZ dimensions

## Defects

The most common defects observed in the laser welds, as shown in Figure 1, are underfill, porosity, sag and lack of penetration. The main reasons for the formation of the underfill defects are the evaporation and expulsion of the molten materials [10]. It was reported that both excessively high and low welding speeds can cause the underfill defect [4, 11]. At a high laser power or low welding speeds (i.e. high heat input), severe material evaporation may result in the formation of the underfill defects [4, 12]. Alternatively, at high welding speeds (low heat input), the rapid cooling rate after welding reduces the solidification time of the FZ and limits flow of the molten weld pool that can render underfill defects [11]. Though underfill defects have been reported to occur on both the top and bottom surfaces of the Ti-6Al-4V welds [4], in the present work the welding conditions resulted in the occurrence of underfill defects almost exclusively on the top surface of the fully penetrated thick gauge section welds, as shown in Figure 1.

The effect of welding speed and defocusing distance on the underfill defect is shown in Figure 3. Both the underfill depth and area increased with increasing welding speed up to a certain limit (1.5 m/min) and then decreased with further increases in the welding speed. The occurrence of a maximum underfill depth and area at an intermediate welding speed (1.5 m/min) can be reasoned on the basis of the combined effects of the evaporation/spatter of the molten weld pool and liquid metal flow that, as mentioned above, are dominant at low and high welding speeds, respectively. In general, underfill defects reduce the weld thickness and work as a stress concentrator, reducing the tensile strength and fatigue life of the welds. Therefore, it is important to avoid or minimize the underfill defect. According to AWS D17.1 [13], the specification for fusion welding for aerospace applications stipulates a maximum underfill depth of  $0.07T$  (where  $T$  is the thickness or 5.1 mm in the present work) for Class A welds. Hence, over the range of welding conditions examined, the autogenous laser welds in Ti6Al4V satisfy Class A requirements in that the underfill discontinuity remained below 0.36 mm ( $0.07 * 5.1$  mm), as indicated by the dashed line in Figure 3a, for all welds with the exception of the specimen T3 (1.5 m/min and -1 mm defocusing distance) that was borderline.

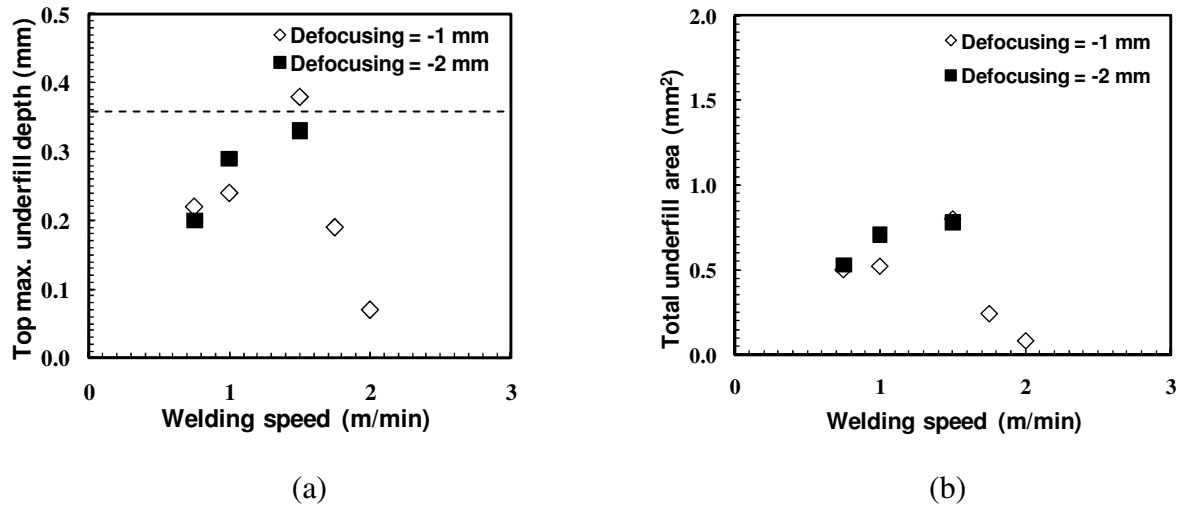


Figure 3 Effect of welding speed and defocusing distance on underfill defect

Porosity formation in the laser welding process is another common concern. The pores can appear at various locations such as near the centerline in the FZ (Figure 4), or close to the FZ/HAZ interface, or randomly scattered in the FZ. In the present work, the occurrence of porosity was mostly observed in the lower half of the FZ. The spherical shape of most of the pores indicates gas type porosity, generally caused by the hydrogen adsorbed in the molten weld pool that cannot escape before solidification. This finding is in agreement with previous work that has related the presence of pores in titanium weldments [14] to hydrogen, particularly because the solubility of hydrogen increases with decreasing temperature in titanium alloys [15]. Moreover, in closely fitted butt welds those are partially penetrated through the thickness of the joint, the propensity for porosity formation increases, as shown in Figure 1-h, since the escape of the gas porosity before solidification is accessible only by means of the top surface. In contrast, for a fully penetrated weld, access to the top and bottom surfaces allows the bubbles to escape more effectively [10]. It is noteworthy also that though the center line porosity is formed due to the evolution of hydrogen at the solid/liquid interface, the porosity in the root area can also be related to the instability of the keyhole [16].

As porosity also decreases the weld cross section and thus the strength of the joint, especially when the pores are large in size and number [10], an analysis of the pore size and porosity area was undertaken in order to understand their evolution with welding speed, as shown in Figure 5. Excluding the welding condition for which a lack of penetration occurred, the general trend for porosity area is a decreasing amount with increasing speed, as indicated in Figure 5a. More porosity is formed at lower welding speed, probably due to longer time available for the growth. Regardless, for the two defocusing conditions studied in this work, it is found that the overall percent porosity area remains below 2% for welding speed between 0.75 – 2.00 m/min as shown in Figure 5b.

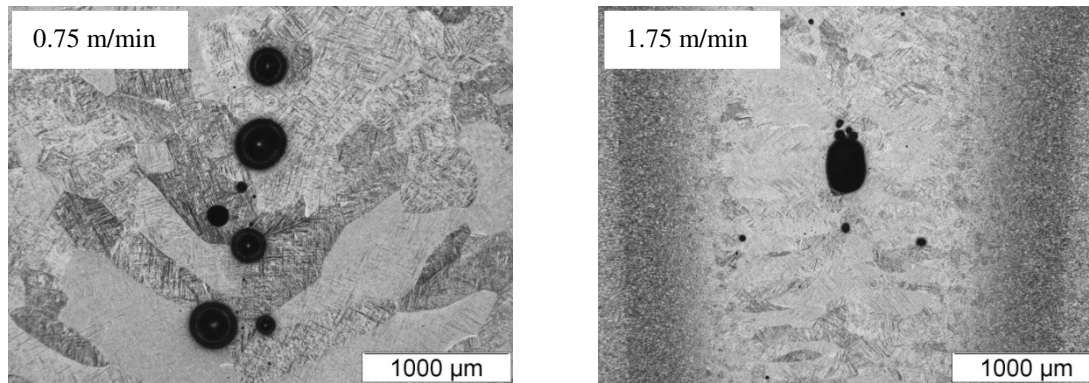


Figure 4 Typical porosity obtained in specimens T1 and T4

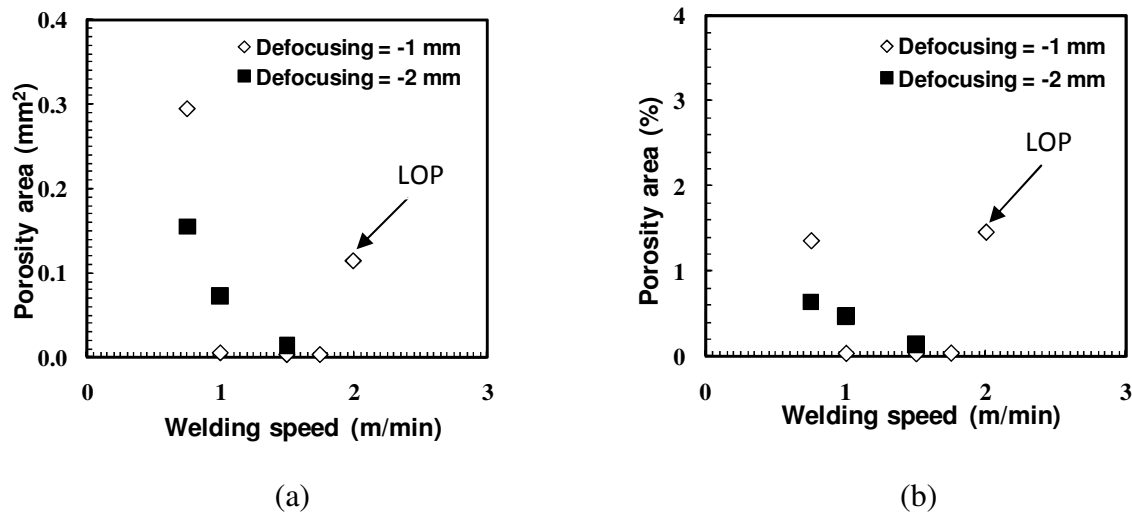


Figure 5 Effect of welding speed on porosity area and percentage of porosity area at two defocusing distances

## Microstructures

The as-received microstructure of mill-annealed Ti-6Al-4V consisted of equiaxed  $\alpha$  with intergranular  $\beta$ . As shown in Figure 6a, the dark regions are intergranular  $\beta$  and the dominating bright regions are equiaxed  $\alpha$ . The  $\beta$  phase is mainly present at the elongated  $\alpha$  grain boundaries. As shown in Figure 1, the FZ macrostructure of the Ti-6Al-4V laser weldments consisted of coarse columnar prior- $\beta$  grains that originate during weld solidification and grow opposite to the heat flow direction [1]. As the FZ prior- $\beta$  grain size increases with increasing heat input during welding, the prior- $\beta$  grain size was observed to decrease with increasing welding speed. The characteristics of microstructure within the prior- $\beta$  grains of the FZ mostly consists of  $\alpha'$  martensite with an acicular morphology (Figure 6c) that is a supersaturated non-equilibrium hexagonal  $\alpha$  phase produced from the diffusionless transformation of the  $\beta$  phase [17, 18]. As vanadium suppresses the martensite formation temperature below room temperature, the FZ microstructure may include some remnant  $\beta$  [19]. The presence of grain boundary  $\alpha$  along the prior- $\beta$  grains (Figure 6c) indicates that the cooling rate is close to the minimum limit necessary for  $\alpha'$  formation, which has been reported to be roughly 410°C/s [20].

The microstructure HAZ on either side of FZ can be easily distinguished in the Ti-6Al-4V weldments, as shown in Figure 1. As the HAZ close to the FZ (near HAZ) experiences higher temperatures during welding than that close to the base metal (far HAZ), the phase constituents were observed to evolve within the HAZ. In particular, the near HAZ region cooled from above the  $\beta$  transus ( $\sim 995^\circ\text{C}$ ) but below the liquidus temperature ( $\sim 1605^\circ\text{C}$ ) and the far HAZ region cooled from below the  $\beta$  transus temperature but above a temperature sufficient to change the microstructure [21]. To this end, the lowest temperature for the far HAZ is difficult to determine as it depends on the transformation kinetics [21]. The near HAZ consisted mainly of  $\alpha'$  with a small amount of primary  $\alpha$ . In contrast, the far HAZ microstructure was a mixture of primary  $\alpha$ , intergranular  $\beta$  phase and  $\alpha'$ , as revealed in Figure 6b. The percentage of  $\alpha'$  decreases from nearly 100% in the near HAZ to zero in the base metal.

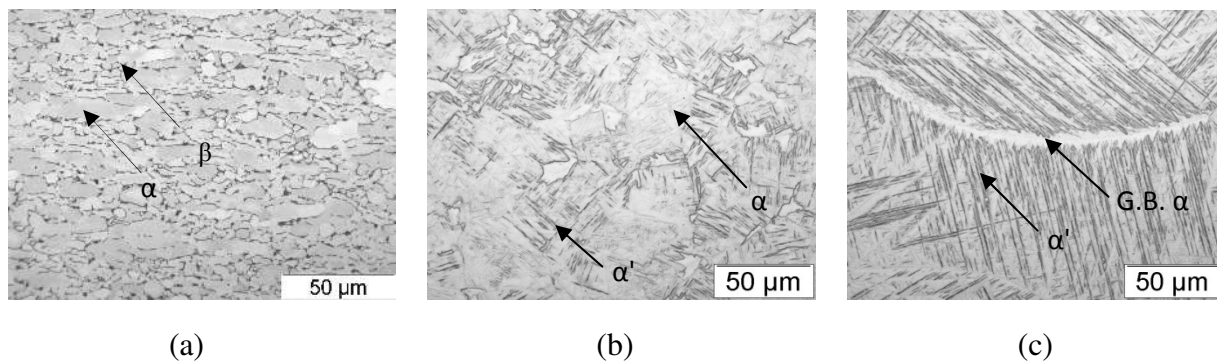


Figure 6 Typical microstructures in (a) base metal (b) middle HAZ and (c) fusion zone

### Micro-Indentation Hardness

Figure 7, the hardness profile of specimen T3, shows that the microhardness behaviour evolves from the lowest values in base metal ( $313 \pm 8$  HV) to the highest values in the FZ ( $361 \pm 10$  HV) of the Ti-6Al-4V weldments. The maximum hardness in the FZ ( $\sim 15\%$  increase relative to base metal) is related to the presence of  $\alpha'$  [4, 12], which exhibits high strength and hardness but at the expense of ductility and toughness [1]. The hardness significantly decreases in the HAZ with the decrease in the amount of  $\alpha'$  from the near HAZ to the far HAZ. The hardness of the near HAZ remains practically similar to that of the FZ due to the dominating presence of the  $\alpha'$  phase in the microstructure. Figure 8 indicates the effect of welding speed on the FZ average hardness. It is found that the average hardness has a trend to increase with increasing welding speed. This is related to the decrease in heat input that increases the cooling rate after welding and results in the formation of more refined  $\alpha'$  with increasing welding speed [21].



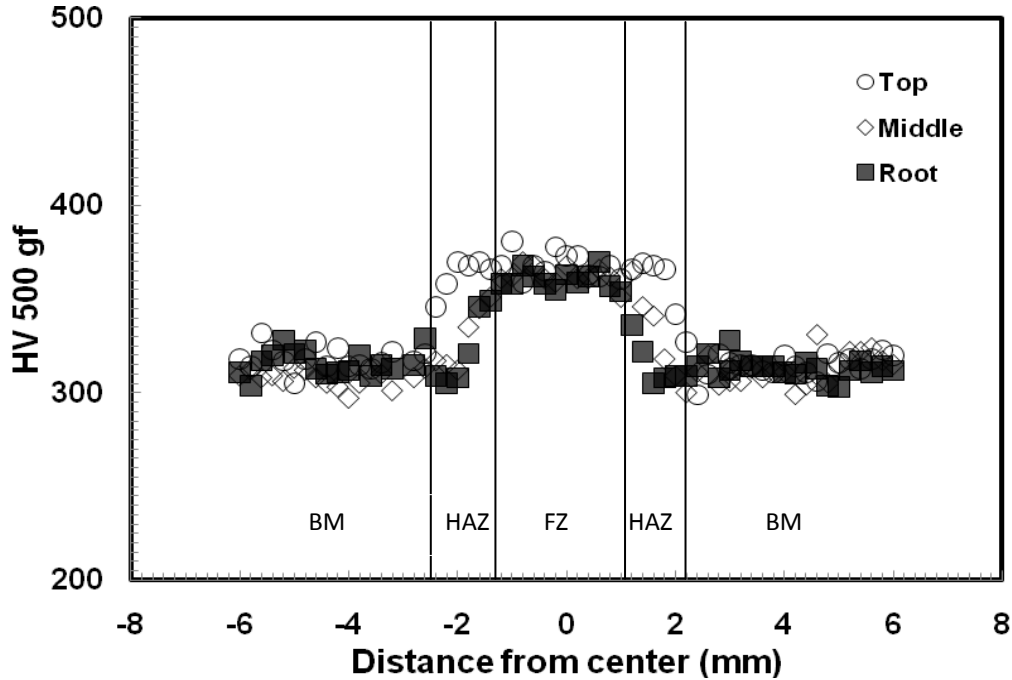


Figure 7 A typical hardness distribution profile (4 kW, 1.5 m/min, -1 mm)

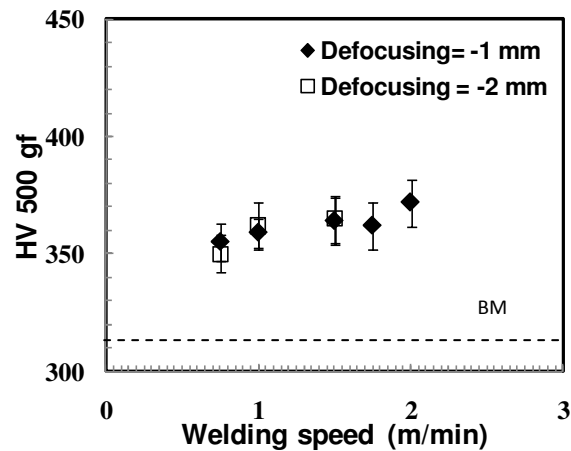


Figure 8 Effect of welding speed and defocusing distance on the average hardness in the FZ

## Conclusions

A continuous wave Nd:YAG laser welding system was used to investigate the butt joint quality of 5.1-mm thick Ti-6Al-4V welded at a laser power of 4 kW, defocusing distances of -1 and -2 mm and various welding speeds (0.75-2.0 m/min). The following conclusions can be drawn:

1. The fusion zone width and area, as well as the HAZ area all decrease with increasing welding speed.

2. Underfill and porosity are the main defects observed in the fully penetrated welds. The maximum underfill depth and area occur at an intermediate welding speed. The porosity area decreases with increasing welding speed.
3. The fusion zone and near HAZ consist mainly of martensite. The far HAZ consists of primary alpha, intergranular beta and martensite. The amount of martensite in the far HAZ decreases from approximately 100% in the near HAZ to zero in the base metal.
4. The fusion zone and the near HAZ have the maximum hardness value due to the presence of the martensite. The hardness in the far HAZ drops sharply with the reduction in the amount of martensite. The average hardness tends to increase with increasing welding speed.
5. No significant differences in weld geometry, underfill defect, microstructure and hardness are observed over the two defocusing distances investigated (-2 mm and -1 mm).

### Acknowledgements

The authors would like to thank Eric Poirier and Xavier Pelletier for their technical assistance during the term of this project.

### References

- [1] ASM, Welding, Brazing, and Soldering, Materials Park, OH: *ASM International*, 1993.
- [2] Z. Sun, D. Pan, and W. Zhang, Correlation Between Welding Parameters and Microstructures in TIG, Plasma, and Laser Welded Ti-6Al-4V, in 6th Int. Conf, *Trends in Welding Research*, Pine Mountain, Georgia, USA, 2002, p 760-767.
- [3] P. Wanjara, M. Brochu, and M. Jahazi, Thin Gauge Titanium Manufacturing Using Multiple-Pass Electron Beam Welding, *Materials and Manufacturing Processes*, vol. 21, 2006, p 439-451.
- [4] X. Cao, and M. Jahazi, Effect of Welding Speed on Butt Joint Quality of Ti-6Al-4V Alloy Welded Using a High-power Nd:YAG Laser, *Optics and Lasers in Engineering*, Vol. 47/11, 2009, p 1231-1241.
- [5] J. Mazumder, and W. M. Steen, Welding of Ti 6Al-4V by a Continuous Wave CO<sub>2</sub> Laser, *Metal Construction*, Vol. 12/9, 1980, p 423-427.
- [6] L. W. Tsay, and C. Y. Tsay, The Effect of Microstructures on the Fatigue Crack Growth in Ti-6Al-4V Laser Welds, *International Journal of Fatigue*, Vol. 19/10, 1997, p 713-720.
- [7] X. Cao, M. Jahazi, J. P. Immarigeon, W. Wallace, A Review of Laser Welding Techniques for Magnesium Alloys, *Journal of Materials Processing Technology*, Vol. 171/2, 2006, p 188-204.
- [8] X. Cao, W. Wallace, C. Poon, J.P. Immarigeon, Research and Progress in Laser Welding of Wrought Aluminum Alloys I. Laser Welding Processes, *Materials Manufacturing Process*, Vol.18/1, 2003 p 1-22.
- [9] ASTM, Metallographic and Materialographic Specimen Preparation, Light Microscopy, Image Analysis and Hardness Testing, *ASTM International*, 2006, p 649.
- [10] C. Dawes, *Laser Welding*, NY: McGraw-Hill, Inc, 1992. p 73

- [11] M. Pastor, H. Zhao, R. P. Martukanitz, T. Debroy, Porosity, Underfill and Magnesium Loss during Continuous Wave Nd:YAG Laser Welding of Thin Plates of Aluminum Alloys 5182 and 5754, *Welding Journal*, 1999, p 207s-216s.
- [12] S. H. Wang, M. D. Wei, and L. W. Tsay, Tensile Properties of LBW Welds in Ti-6Al-4V Alloy at Evaluated Temperatures Below 450°C, *Materials Letters*, Vol. 57/12, 2003, p 1815-1823.
- [13] AWS, Specification for Fusion Welding for Aerospace Application, *American Welding Society*, 2001.
- [14] Z. Khaled, An Investigation of Pore Cracking in Titanium Welds, *Journal of Materials Engineering and Performance*, Vol. 3/3, 1994, p 419-434.
- [15] D. R. Mitchell, Porosity in Titanium Welds, *Welds J.*, Vol. 61, 1982, p 157s-167s.
- [16] M. Pastor, H. Zhao, and T. Debroy, Pore Formation During Continuous Wave Nd:YAG Laser Welding of Aluminum for Automotive Applications, *Revista de Metalurgia*, vol. 36/2, 2000 p 108-117.
- [17] J. W. Elmer, T. A. Palmer, S. S. Babu, W. Zhang, T. Debroy, Phase Transformation Dynamics During Welding of Ti-6Al-4V, *Journal of Applied Physics*, vol. 95/12, 2004.
- [18] G. Lutjering, and J. C. Williams, *Titanium*, 2 ed.: Springer, 2007.
- [19] M. J. Donachie, *Titanium: A Technical Guide*, , ASM International, Materials Park, OH, 1989.
- [20] T. Ahmed, and H. J. Rack, Phase Transformations During Cooling in  $\alpha + \beta$  Titanium Alloys, *Materials Science & Engineering A*, Vol. 243, 1998, p 206-211.
- [21] A. B. Short, Gas Tungsten Arc Welding of  $\alpha + \beta$  Titanium Alloys: A Review, *Materials Science and Technology*, Vol. 25, 2009 p 309-324.